Active Vibration and Noise Control of a Car Engine: Modeling and Experimental Validation

Ulrich Gabbert and Stefan Ringwelski

Abstract The paper presents an overall design approach for smart light-weight structures made of metal sheets or fiber reinforced plastics, equipped with thin piezoelectric wafers as actuators and sensors to control vibration and noise. The design process is based on an overall finite element model, which includes the passive structure, the piezoelectric wafers attached to the structure or embedded between the layers of a composite and the controller as well. In active noise control the vibrating structure interacts with the surrounding fluid, which is also included into the overall model. In order to evaluate the quality of the approach, test simulations are carried out and the results are compared with experimental data. As a test case, a smart car engine with surface-mounted piezoelectric actuators and sensors for active noise reduction is considered. A comparison between the measured values and those predicted by the coupled finite element model shows a good agreement.

1 Introduction

In the past years, significant progress has been made in the field of vibration and noise control in automotive engineering. The control of noise and vibration is essential in the design process of an automobile, since it contributes to comfort, efficiency and safety. There are two different approaches to achieve noise and vibration attenuation. In the widely used first approach the vibration and the sound emission of structures are reduced passively by modifying the structural geometry or by applying additional damping materials. These methods are best suited to a frequency range above 1,000 Hz. The second approach is the application of active control techniques to reduce unwanted structural vibration and noise. These

U. Gabbert (✉) · S. Ringwelski
Institute of Mechanics, Otto-von-Guericke University of Magdeburg, Magdeburg, Germany
e-mail: ulrich.gabbert@ovgu.de; stefan.ringwelski@ovgu.de

Alexander K. Belyaev et al. (eds.), *Mechanics and Model-Based Control of Advanced Engineering Systems*, DOI 10.1007/978-3-7091-1571-8_14,

techniques are usually employed in a frequency range between 50 and 1,000 Hz. In active noise reduction usually smart materials are attached to structures as actuators and sensors connected by a control unit which enables the system to reduce structural vibrations with the objective to reduce simultaneously also the sound radiation caused by structural vibrations.

Considering passenger cars, the power train represents one of the main noise sources, especially during idling, slow driving speeds and full load acceleration. One major contributor to the overall power train noise emission is the engine oil pan. Therefore, the paper aims to design a smart car engine with piezoelectric actuators and sensors attached on the surface of the oil pan for active noise reduction.

Over the past years, some researchers have already studied active noise reduction approaches at car oil pans [16] and a truck oil pans [5] using distributed piezoelectric actuators. However in these studies, the oil pan was treated separately and no attempt was made to consider the interactions between the crankcase and the oil pan. Naake et al. [13] employed piezoceramic patch actuators to minimize the vibrations of a car windshield. The goal of this control approach was to achieve a reduced acoustic pressure level inside the cabin. For the same reasons a similar approach was adopted by Weyer and Monner [20] and Nestorović et al. [14].

The development and industrial application of smart systems for active noise and vibration control require efficient and reliable simulation tools. Virtual models are of particular interest in the design process, since they enable the testing of several control strategies and they are required to determine optimal sensor and actuator locations. There are several numerical approaches [6,7,10,11,21] available for predicting the behavior of active systems, which include the modeling of the mechanical structure, the piezoelectric actuators and sensors, the surrounding fluids as well as the applied control algorithm.

In the present paper an overall finite element approach is proposed. For modeling thin walled structures shell elements are used, the piezoelectric patches are modelled with special electromechanical coupled shell elements, and the acoustic fluid is modelled with 3D fluid elements, which include the coupling conditions with the structural shell elements. The far field is described with infinite elements developed on the basis of the doubly asymptotic approximation [4]. This approach results in a symmetric form of the coupled electro-mechanical-acoustic system of the equations of motion, including the electric potential, the displacements and the velocity potential as nodal degrees of freedom.

For controller design purposes a reduced model is derived based on selected structural and acoustic eigenmodes.

In order to check the validity of the approach, numerical and experimental studies are carried out using a car engine with surface-mounted piezoelectric actuators. The simulated and the measured data are in a good agreement showing that the developed overall simulation approach can be used for industrial design purposes.

Finally, the quality of the designed active oil pan is checked by experimental testing on a fired engine using a dSPACE controller board which determines the necessary control outputs for the actuators. In the experiment, engine run ups are measured on an engine test bench for the uncontrolled and controlled case.

2 Finite Element Modeling

2.1 Finite Element Model of Piezoelectric Shell Structures

In this section, a simple piezoelectric composite Mindlin-type shell element for analyzing laminated plates with integrated piezoelectric actuators and sensors is briefly discussed. More details regarding the development and the implementation of this finite element can be found in [17] and [3].

In the shell element, it is assumed that the thickness of the layers is the same at each node and the deformations are small. Additionally, it is presumed that the modeled composite laminate plate consists of perfectly bonded layers and the bonds are infinitesimally thin as well as nonshear-deformable. The shell element has six degrees of freedom $u_1, u_2, u_3, \theta_{x2}, \theta_{x1}, \theta_{x3}$ at each node for describing the elastic behavior and additionally one electric potential degree of freedom per layer to model the piezoelectric effect. The strain displacement relations for the used plane shell element are based on the Mindlin first order shear deformation theory.

The poling direction of the piezoelectric layers is assumed to be coincident with the thickness direction, which means that the electric field acts only perpendicular to the layers. Moreover, the difference in the electric potential φ is supposed to be constant in each layer of the shell element. The electric field, which varies linearly through the thickness of a piezoelectric layer, causes an in-plane expansion or contraction. Thus, for modeling the electric field only one electric degree of freedom per layer has to be specified within the element. In Marinković et al. [12] it is shown, that these assumptions are accurate enough in thin structure applications.

The coupled electromechanical behavior of piezoelectric materials in a low voltage regime can be modeled with sufficient accuracy by means of the linearized constitutive equations. In matrix form, the constitutive relations for a piezoelectric layer are defined as [15]

$$\boldsymbol{\sigma} = \mathbf{Q}\boldsymbol{\varepsilon} - \mathbf{e}E\,, \quad D = \mathbf{e}^T\boldsymbol{\varepsilon} + \boldsymbol{\kappa}E. \tag{1}$$

Here σ denotes the stress vector, D is the dielectric displacement in thickness direction, $\mathbf{Q}$ and $\mathbf{e}$ are the plane-stress reduced elastic stiffness and the piezoelectric matrices, respectively. The coefficient $\boldsymbol{\kappa}$ represents the plane-stress reduced dielectric permittivity of the piezoelectric layer and E is the electric field of the shell element. The piezoelectric constitutive relations given above are used within the weak form of the mechanical equilibrium equations [19] to derive the electromechanical FE equations of a piezoelectric layer by applying a standard Galerkin procedure. After adding the local equations of all layers and elements to a global model, the resulting system of coupled algebraic equations can be expressed as

$$\begin{bmatrix} \mathbf{M}_u & \mathbf{0} \\ \mathbf{0} & \mathbf{0} \end{bmatrix} \begin{bmatrix} \ddot{\mathbf{u}} \\ \ddot{\boldsymbol{\varphi}} \end{bmatrix} + \begin{bmatrix} \mathbf{C}_u & \mathbf{0} \\ \mathbf{0} & \mathbf{0} \end{bmatrix} \begin{bmatrix} \dot{\mathbf{u}} \\ \dot{\boldsymbol{\varphi}} \end{bmatrix} + \begin{bmatrix} \mathbf{K}_u & \mathbf{K}_{u\varphi} \\ \mathbf{K}_{u\varphi}^T & -\mathbf{K}_{\varphi} \end{bmatrix} \begin{bmatrix} \mathbf{u} \\ \boldsymbol{\varphi} \end{bmatrix} = \begin{bmatrix} \mathbf{f}_u \\ \mathbf{f}_{\varphi} \end{bmatrix}, \tag{2}$$

where $\mathbf{u}$ is the vector with the nodal structural displacements, and $\boldsymbol{\varphi}$ is the vector with the nodal values of the electric potentials. The matrices $\mathbf{M}_u$, $\mathbf{K}_u$ and $\mathbf{K}_\varphi$ are the structural mass, the structural stiffness and the dielectric matrix, respectively. The piezoelectric coupling arises in the piezoelectric coupling matrix $\mathbf{K}_{u\varphi}$. For convenience, a Rayleigh damping is introduced into the system of Eqs. (2), assuming that the matrix $\mathbf{C}_u$ is a linear combination of the matrices $\mathbf{M}_u$ and $\mathbf{K}_u$. The external loads are stored in the mechanical load vector $\mathbf{f}_u$ and in the electric load vector $\mathbf{f}_\varphi$. In the following, it is assumed that the vector $\mathbf{u}$ contains the entire nodal displacements of the mechanical structure as well as the piezoelectric actuators and sensors.

2.2 Finite Element Modeling of the Acoustic Fluid

In this section, a FE formulation is presented to model the finite fluid domains around the smart shell structure. The homogeneous and inviscid acoustic fluid is modeled by using the linear acoustic wave equation [8]

$$\frac{1}{c^2}\ddot{\Phi} - \Delta\Phi = 0. \tag{3}$$

In the present study, a hexahedron element is chosen to discretize the fluid domains. The velocity potential is considered as the nodal degree of freedom in the finite element instead of the acoustic pressure p, since Everstine [2] has recommended introducing the velocity potential Φ as a new degree of freedom in order to get symmetric matrices. In Eq. (3) Δ is the Laplacian operator and c is the speed of sound.

To take into account an infinite outer fluid region, the doubly asymptotic approximation [4] is used. The behavior of the outer fluid is considered only in the low and the high frequency range. At low frequencies the fluid of the outer region is assumed to be incompressible, and in the high frequency range plane waves are considered.

Following the standard finite element procedure, the matrix equation of the discretized fluid domain becomes

$$\mathbf{M}_a\ddot{\boldsymbol{\Phi}} + (\mathbf{C}_a + \mathbf{C}_0)\dot{\boldsymbol{\Phi}} + (\mathbf{K}_a + \mathbf{K}_0)\boldsymbol{\Phi} = \mathbf{f}_a, \tag{4}$$

with the acoustic mass matrix $\mathbf{M}_a$, the acoustic damping matrix $\mathbf{C}_a$, the acoustic stiffness matrix $\mathbf{K}_a$, the acoustic load vector $\mathbf{f}_a$, and the matrices $\mathbf{C}_0$ and $\mathbf{K}_0$, which are additional matrices taking into account the coupling with special infinite or semi-infinite fluid elements for describing the fare field. For more details see Lefèvre [9]. Similar coupling terms also occur if the fare field is described with boundary elements, which can also be coupled with 3D fluid finite elements applied for approximating the near field [17].

2.3 The Vibro-Acoustic Coupling

The dynamic behavior of thin lightweight structures with fluid loading is strongly affected by the interaction between the subsystems. The purpose of the following section is to present a overall FE approach to model the coupling that occurs in smart systems with a fluid-structure interface.

The acoustic pressure represents an additional surface distributed load acting normal to the surface of the piezoelectric structure, such resulting in an additional load vector $\mathbf{f}_{uc}$, which appears on the right hand side of Eq. (3). This additional load vector acting at the fluid-structure interface can be expressed as

$$\mathbf{f}_{uc} = \mathbf{C}_{uc}\dot{\boldsymbol{\Phi}}, \tag{5}$$

where $\mathbf{C}_{uc}$ is the coupling matrix at the fluid-structure interface. In an analogous manner, the vibrating structure interacts with the fluid. This influence is described by an additional load vector $\mathbf{f}_{ac}$, which appears on the right hand side of Eq. (4). This new acoustic load vector can be expressed by an expression similar to Eq. (5) as

$$\mathbf{f}_{ac} = -\frac{1}{\rho_0}\mathbf{C}_{uc}\dot{\mathbf{u}}, \tag{6}$$

with $\mathbf{C}_{uc}$ as the coupling matrix regarding structural vibrations. The variable ρ_0 stands for the density of the acoustic medium.

Equations (2) and (4) are coupled by introducing the Eqs. (5) and (6), which results in symmetric matrices by multiplying all lines related to the fluid degrees of freedom with $(-\rho_0)$. If the element matrices are assembled into the global system matrices, the semi discrete form of the equation of motion of the coupled electro-mechanical-acoustic field problem can be written as

$$\begin{bmatrix} \mathbf{M}_u & \mathbf{0} & \mathbf{0} \\ \mathbf{0} & \mathbf{0} & \mathbf{0} \\ \mathbf{0} & \mathbf{0} & -\rho_0\mathbf{M}_a \end{bmatrix} \begin{bmatrix} \ddot{\mathbf{u}} \\ \ddot{\boldsymbol{\varphi}} \\ \ddot{\boldsymbol{\Phi}} \end{bmatrix} + \begin{bmatrix} \mathbf{C}_u & \mathbf{0} & -\mathbf{C}_{uc} \\ \mathbf{0} & \mathbf{0} & \mathbf{0} \\ -\mathbf{C}_{uc}^T & \mathbf{0} & -\rho_0\left(\mathbf{C}_a + \mathbf{C}_0\right) \end{bmatrix} \begin{bmatrix} \dot{\mathbf{u}} \\ \dot{\boldsymbol{\varphi}} \\ \dot{\boldsymbol{\Phi}} \end{bmatrix}$$
$$+ \begin{bmatrix} \mathbf{K}_u & \mathbf{K}_{u\varphi} & \mathbf{0} \\ \mathbf{K}_{u\varphi}^T & -\mathbf{K}_\varphi & \mathbf{0} \\ \mathbf{0} & \mathbf{0} & -\rho_0\left(\mathbf{K}_a + \mathbf{K}_0\right) \end{bmatrix} \begin{bmatrix} \mathbf{u} \\ \boldsymbol{\varphi} \\ \boldsymbol{\Phi} \end{bmatrix} = \begin{bmatrix} \mathbf{f}_u \\ \mathbf{f}_\varphi \\ -\rho_0\mathbf{f}_a \end{bmatrix}. \tag{7}$$

3 Controller Design

The numerical simulation of smart structures within the finite element frame requires an overall finite element model including the passive structure with the surrounding fluid, the active sensor and actuator elements, as well as an appropriate

model of the controller. For the controller design numerous techniques are at disposal, and the application of an appropriate control law is closely related to the requirements of the specific problem. For a model based controller design the large finite element models have to be reduced. One of the standard techniques is the modal reduction based on preselected eigenmodes of the system. To apply this technique, the coupled system of motion (7) is rewritten in the following compact form

$$\tilde{\mathbf{M}}\ddot{\mathbf{r}} + \tilde{\mathbf{C}}\dot{\mathbf{r}} + \tilde{\mathbf{K}}\mathbf{r} = \tilde{\mathbf{f}}, \tag{8}$$

Introducing the state space vector

$$\mathbf{z} = \begin{bmatrix} \mathbf{r} & \dot{\mathbf{r}} \end{bmatrix}^T = \begin{bmatrix} \mathbf{u} & \boldsymbol{\varphi} & \boldsymbol{\Phi} & \dot{\mathbf{u}} & \dot{\boldsymbol{\varphi}} & \dot{\boldsymbol{\Phi}} \end{bmatrix}^T, \tag{9}$$

from Eq. (9) it follows

$$\begin{bmatrix} \tilde{\mathbf{C}} & \tilde{\mathbf{M}} \\ \tilde{\mathbf{M}} & \mathbf{0} \end{bmatrix} \dot{\mathbf{z}} + \begin{bmatrix} \tilde{\mathbf{K}} & \mathbf{0} \\ \mathbf{0} & -\tilde{\mathbf{M}} \end{bmatrix} \mathbf{z} = \tilde{\mathbf{B}}\dot{\mathbf{z}} + \tilde{\mathbf{A}}\mathbf{z} = \begin{bmatrix} \tilde{\mathbf{f}} \\ \mathbf{0} \end{bmatrix}. \tag{10}$$

From Eq. (10) the linear eigenvalue problem can be derived as

$$\left(\tilde{\mathbf{A}} - \lambda_j \tilde{\mathbf{B}}\right) \hat{\mathbf{z}}_j = \mathbf{0}. \tag{11}$$

The solution of Eq. (11) results in the modal matrix $\mathbf{Q}$ with $2k$ pairs of conjugate complex eigenvectors

$$\mathbf{Q} = \begin{bmatrix} \hat{\mathbf{z}}_1 & \hat{\mathbf{z}}_2 & \dots & \hat{\mathbf{z}}_{2k} \end{bmatrix}. \tag{12}$$

If the modal matrix $\mathbf{Q}$ is ortho-normalized with $\mathbf{Q}^T\tilde{\mathbf{B}}\mathbf{Q} = \mathbf{I} = diag(1)$ and $\mathbf{Q}^T\tilde{\mathbf{A}}\mathbf{Q} = \boldsymbol{\Lambda} = diag(\Lambda)$, and new coordinates $\mathbf{z} = \mathbf{Q}\mathbf{q}$ are introduced in Eq. (12), the reduced state space form is obtained as

$$\dot{\mathbf{q}} + \boldsymbol{\Lambda}\mathbf{q} = \mathbf{Q}^T \begin{bmatrix} \tilde{\mathbf{f}} \\ \mathbf{0} \end{bmatrix}. \tag{13}$$

If the right hand side of Eq. (13) is subdivided into the control forces and the external forces and the measurement equation (15) is added, the following set of equations, which can be used to design an appropriate controller, is obtained as

$$\dot{\mathbf{q}} = -\boldsymbol{\Lambda}\mathbf{q} + \mathbf{Q}^T \begin{bmatrix} \bar{\mathbf{B}} \\ \mathbf{0} \end{bmatrix} \mathbf{u}(t) + \mathbf{Q}^T \begin{bmatrix} \bar{\mathbf{E}} \\ \mathbf{0} \end{bmatrix} \mathbf{f}(t) = \mathbf{A}\mathbf{q} + \mathbf{B}\mathbf{u}(t) + \mathbf{E}\mathbf{f}(t), \tag{14}$$

$$\mathbf{y}(t) = \mathbf{C}\mathbf{q} + \mathbf{D}\mathbf{u}(t) + \mathbf{F}\mathbf{f}(t). \tag{15}$$

For controller design purposes the state matrices **A**, **B**, **E**, **C**, **D** and **F** are transferred from the finite element approach to Matlab/Simulink via an internal data interface. Based on the model matrices different controller, such as the velocity feedback control, the optimal LQ control and the modal reference adaptive control (MRAC) have been developed and successfully tested.

4 Smart Car Engine for Active Noise Reduction

The purpose of this section is to demonstrate the applicability of the proposed modeling approach. For this reason, a smart car engine that consists of a crankcase an oil pan with surface-mounted piezoelectric actuators and sensors for active noise reduction is designed.

4.1 Dominant Mode Shapes

In order to design a smart stripped car engine for active noise and vibration control, it is essential to identify the most dominant mode shapes. This step is carried out by means of harmonic FE simulations using a Fourier transformed version of Eq. (2).

A point force excitation at the oil pan flange is chosen to excite all eigenmodes in a frequency range up to 1,200 Hz. Figure 1 shows the resulting frequency response function (FRF) between the structural displacement at the center of the oil pan bottom and the excitation force at the flange. In addition, the mode shapes that are associated with the respective resonance frequencies are illustrated. In Fig. 1, it can be seen that the first and the third eigenmode are pure bending modes of the oil pan bottom. The second and the fourth mode are global bending modes of the whole stripped car engine. Under real operating conditions these bottom modes are the main contributor to the overall sound emission. Due to this fact, the present approach aims to control only these modes.

4.2 Definition of the Actuator Positions and Modeling

An often used method for the actuator placement is based on the assumption that an actuator is placed well when it is able to influence significantly the shape of the structural modes. This means that an in-plane actuator should be placed at positions on the surface of the structure, where the strains and the corresponding electric potentials are the highest [1, 18]. In case of the stripped car engine, the first and the third eigenmode are considered. The modal strains of these modes can be derived from the structural part $\hat{\mathbf{u}}_j$ of the complex eigenvectors $\hat{\mathbf{z}}_j$ with $j = 1$ and 3.

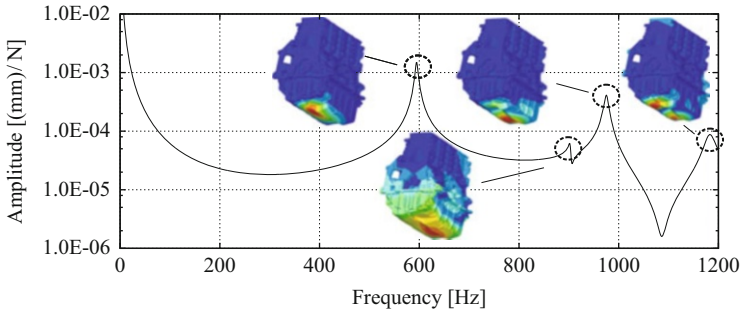

Fig. 1 Computed FRF of the stripped car engine

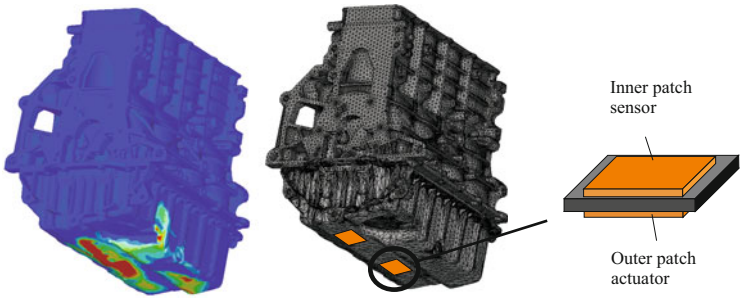

Fig. 2 Contour plot of the superposed field and FE mesh with selected actuator and sensor position

The structural displacements $\hat{\mathbf{u}}_j$ are associated with the modal strains $\hat{\boldsymbol{\varepsilon}}_j$ by the relationship

$$\hat{\boldsymbol{\varepsilon}}_j = \mathbf{B}_u \hat{\mathbf{u}}_j , \tag{16}$$

where $\mathbf{B}$ is the matrix that calculates the strains of a finite element surface area using nodal displacements. The modal strains $\hat{\boldsymbol{\varepsilon}}_j$ are related with the electric potentials $\hat{\varphi}_j$ by the constitutive equations of piezoelectricity [17]. By means of a multiplicative superposition of the electric potentials $\hat{\varphi}_j$ one obtains the super-posed field

$$\hat{\varphi}_{max} = \prod_{j=1,3} \hat{\varphi}_j . \tag{17}$$

In contrast to an additive superposition, the multiplicative superposition makes sure that the actuators are not placed on node lines. A contour plot of the super-posed field $\hat{\varphi}_{max}$ allows the definition of optimal actuator positions. Two actuator positions have been selected according to the contour plot visible in Fig. 2 (picture at the left hand side), where the orange areas mark the preferred regions for placing actuators. The orange rectangular areas of the FE mesh (picture in the center of

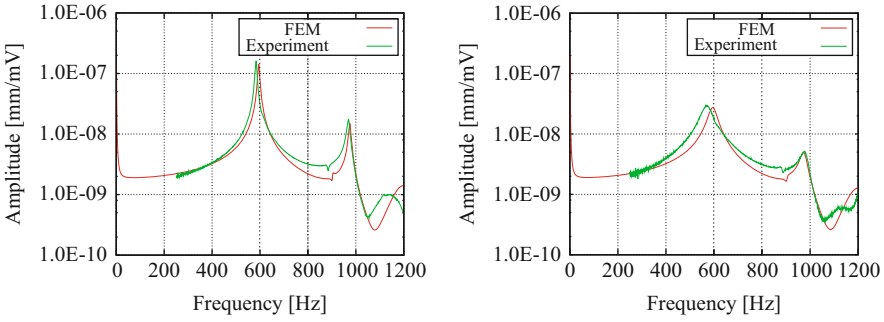

Fig. 3 Uncontrolled (*left*) and controlled (*right*) FRFs of the stripped car engine

Fig. 2) mark the two selected actuator positions. Additionally, two sensors are placed on the opposite side of the oil pan. The collocated design of the piezoelectric actuator/sensor pairs guarantees control stability. It should be noted that more than two collocated actuator/sensor pairs are possible.

4.3 Numerical and Experimental Studies

In the following section numerical simulations are carried out and the results are compared with experimental data to test the performance of the system designed. In the analysis the piezoceramic actuators and sensors are modeled using multilayer shell elements. A velocity feedback control is chosen to compute input signals for the actuators that are bonded on the outer surface of the oil pan. Standard tetrahedral elements are used to model the irregular-shaped geometry of the crankcase and the oil pan. The surrounding fluid volume is approximated with a mixture of tetrahedral and hexahedral elements. These elements are coupled by the above presented fluid-structure coupling matrices with the structural finite elements used for modeling the engine. For the far field approximation the above mentioned infinite elements are applied. In all these elements, quadratic shape functions are employed. Figure 2 illustrates the structural FE mesh of the stripped car engine.

For comparison purposes uncontrolled and controlled FRFs are considered. Similar to the computations in Sect. 4.1 a harmonic point force excitation at the oil pan flange has been used to excite the system, and the response is regarded in terms of the structural displacement at the center of the oil pan bottom. In Fig. 3, it can be observed that the measured data and the numerical predictions agree very well. Additionally, the results in Fig. 3 show that a significant damping at the dominating resonance frequencies is achieved, due to the implementation of the velocity feedback control. The amplitudes are reduced by more than 14 dB at 595 Hz and by about 10 dB at 975 Hz.

Figure 4 shows the deformed shape of the car engine for the uncontrolled and the controlled case at the first resonance frequency (595 Hz). It can be seen that

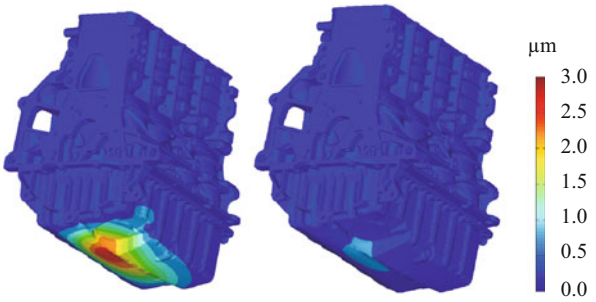

Fig. 4 Uncontrolled (*left*) and controlled (*right*) deformed shape of the stripped car engine at the first eigenfrequency

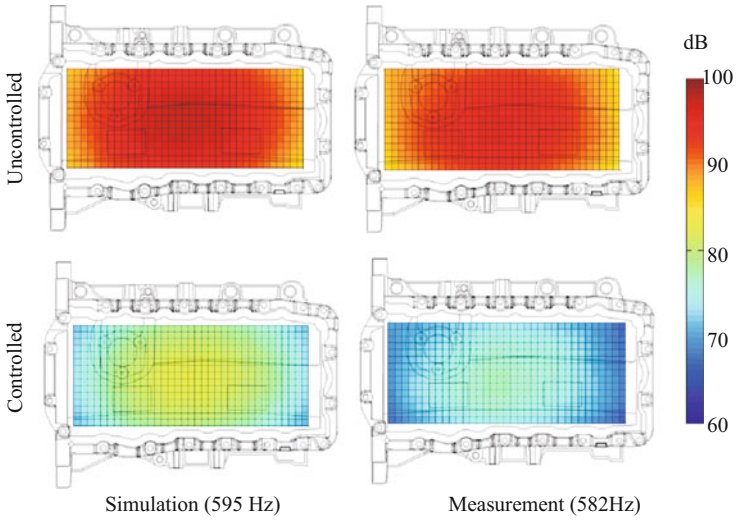

Fig. 5 Sound pressure distribution of the controlled and uncontrolled stripped engine

the displacements are reduced by approximately 16 dB. In order to analyze the near-field airborne noise from the outer surface of the oil pan, the corresponding pressure fields are computed. On the left-hand side of Fig. 5 the computed sound pressure distribution of the uncontrolled and controlled stripped engine are plotted. For visualization a plane approximately 50 mm apart from the bottom surface was chosen. To verify the simulated data, measurements have been carried out in a free-field room with the help of a uniformly distributed microphone-array. The acoustic field of the structure was scanned at 32 microphone positions with 50 mm measuring grid spacing between. The corresponding measurements are shown on the right-hand side of Fig. 5. From Fig. 5 can be seen that the simulation results correlate

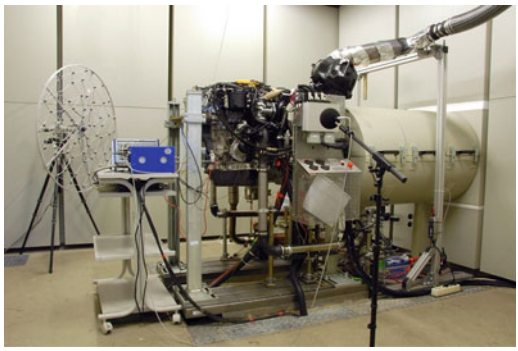

Fig. 6 Four-cylinder diesel engine in an anechoic room

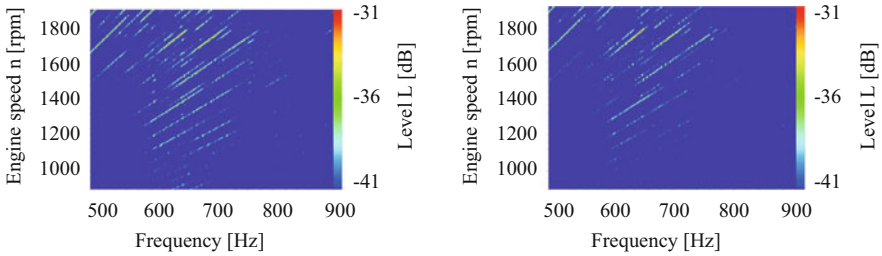

Fig. 7 Campbell diagrams of the uncontrolled (*left*) and controlled (*right*) diesel engine

well with the experimental results. Furthermore it can be noticed that due to the controller influence the sound pressure level is reduced by approximately 16 dB, which indicates the noise reduction potential of the designed system.

4.4 Engine Measurements on a Test Bench

In order to evaluate the quality of the smart system designed, several experimental tests on an acoustic engine test bench have been carried out under real operating conditions. In Fig. 6 the altered four-cylinder common rail diesel engine is shown.

In order to get an overview of the uncontrolled and controlled behavior at higher engine speeds, engine run-ups (900–3,000 rpm) were made and evaluated by means of appropriate Campbell diagrams. A displacement patch sensor was used to generate the diagrams, since this sensor represents the entire vibration characteristics of the oil pan. The measurements, shown in Fig. 7, reveal that due to the controller influence the displacement level amplitudes in the resonance frequency regions are reduced by approximately 4 dB, which indicates the noise reduction potential of the designed system.

5 Conclusions

In this paper, a coupled FE formulation has been presented to simulate a fluid-loaded smart lightweight structure with surface-mounted piezoelectric actuators and sensors. Besides the passive structure, the finite element model includes active piezoelectric elements, the acoustic fluid, the vibro-acoustic coupling and the controller influence as well. Piezoelectric layered shell type finite elements have been extended to include the vibro-acoustic coupling with 3D acoustic finite elements and infinite elements for the far field. Because of the large number of degrees of freedom of the FE model a modal truncation technique based on a complex eigenvalue analysis is performed. The reduced model is transformed into the state space form. The developed approach is applied to design the smart car engine. For the design process structural FE simulations of the car engine were carried out to identify the most dominant mode shapes within a frequency range of 0–1,200 Hz. Based on these results optimal actuator positions were calculated. Additionally, the exterior noise radiation of a stripped car engine was numerically analyzed by applying a mixture of finite and infinite elements. A velocity feedback control algorithm in a real collocated design was used to obtain a high active damping effect. To demonstrate the applicability and validity of the developments, test simulations are carried out, which were compared with measurements performed on a laboratory set-up. This comparison between the experimental and numerical results shows a good agreement. In order to demonstrate that the designed system works also under real operating conditions tests on a fired engine have been carried out. With a velocity feedback control, attenuations up to 4 dB in the vibration level were achieved at the resonance frequency regions of the most dominant modes.

References

1. Bin, L., Yugang, L., Xuegang, Y., Shanglian, H.: Maximal modal force rule for optimal placement of point piezoelectric actuators for plates. J. Intell. Mater. Syst. Struct. **11**(7), 512–515 (2000)
2. Everstine, G.C.: Finite element formulations of structural acoustics problems. Comput. Struct. **65**(3), 307–321 (1997)
3. Gabbert, U., Berger, H., Köppe, H., Cao, X.: On modelling and analysis of piezoelectric smart structures by the finite element method. Appl. Mech. Eng. **5**(1), 127–142 (2000)
4. Geers, T.L.: Doubly asymptotic approximations for transient motions of submerged structures. J. Acoust. Soc. Am. **64**(5), 1500–1508 (1978)
5. Heintze, O., Misol, M., Algermissen, S., Hartung, C.F.: Active structural acoustic control for a serial production truck oil pan: experimental realization. In: Proceedings of the Adaptronic Congress, Berlin, pp. 147–153 (2008)
6. Kaljević, I., Saravanos, D.A.: Steady-state response of acoustic cavities bounded by piezoelectric composite shell structures. J. Sound Vib. **204**(3), 459–476 (1997)
7. Khan, M.S., Cai, C., Hung, K.C., Varadan, V.K.: Active control of sound around a fluid-loaded plate using multiple piezoelectric elements. Smart Mater. Struct. **11**, 346–354 (2002)

8. Kollmann, F.G.: Maschinenakustik. Grundlagen, Meßtechnik, Berechnung, Beeinflussung. Springer, Berlin (2000)
9. Lefèvre, J.: Finite element simulation of adaptive light-weight structures for vibration and noise reduction (in German). VDI Verlag, Düsseldorf (2007)
10. Lefèvre, J., Gabbert, U.: Finite element modelling of vibro-acoustic systems for active noise reduction. Technol. Mech. **25**(3–4), 241–247 (2005)
11. Lerch, R., Landes, H., Friedrich, W., Hebel, R., Hoss, A., Kaarmann, H.: Modelling of acoustic antennas with a combined finite-element-boundary-element method. In: Proceedings of the IEEE Ultrasonics Symposium, Tucson, pp. 643–654 (1992)
12. Marinković, D., Köppe, H., Gabbert, U.: Numerically efficient finite element formulation for modeling active composite laminates. Mech. Adv. Mater. Struct. **13**, 379–392 (2006)
13. Naake, A., Schmidt, K., Meschke, J., Weyer, T., Knorr, A., Weiser, J., Rehfeld, M., Rödig, T.: Vehicle windshield with active noise reduction. In: Proceedings of the Adaptronic Congress, Göttingen, vol. 22, pp. 1–5 (2007)
14. Nestorović, T., Seeger, F., Köppe, H., Gabbert, U.: Controller design for the active vibration suppression of a car roof. In: Proceedings of the International Congress Motor Vehicles & Motors, Kragujevac (2006)
15. Pinto Correia, I.F., Mota Soares, C.M., Mota Soares, C.A., Normam, J.H.: Active control of axisymmetric shells with piezoelectric layers: a mixed laminated theory with a high order displacement field. Comput. Struct. **80**(1/2), 2265–2275 (2002)
16. Redaelli, M., Manzoni, S., Cigada, A., Wimmel, R., Siebald, H., Fehren, H., Schiedewitz, M., Wolff, K., Lahey, H.-P., Nussmann, C., Nehl, J., Naake, A.: Different techniques for active and passive noise cancellation at powertrain oil pan. In: Proceedings of the Adaptronic Congress, Göttingen, vol. 21, pp. 1–8 (2007)
17. Ringwelski, S., Gabbert, U.: Modeling of a fluid-loaded smart shell structure for active noise and vibration control using a coupled finite element-boundary element approach. Smart Mater. Struct. **19**(10), 105009 (2010)
18. Seeger, F.: Simulation und Optimierung adaptiver Schalenstrukturen. VDI Verlag, Düsseldorf (2004)
19. Verhoosel, C.V., Gutierrez, M.A.: Modelling inter- and transgranular fracture in piezoelectric polycrystals. Eng. Fract. Mech. **76**(6), 742–760 (2009)
20. Weyer, T., Monner, H.P.: PKW-Innenlärmreduzierung durch aktive Beruhigung der durch die Motorharmonischen erregten Dachblech-Schwingungen. Motor und Aggregateakustik (2003)
21. Zhang, Z., Chen, Y., Yin, X., Hua, H.: Active vibration isolation and underwater sound radiation control. J. Sound Vib. **318**, 725–736 (2008)